Journal of King Saud University - Science 35 (2023) 102958

HOSTED BY

Contents lists available at ScienceDirect

Journal of King Saud University - Science

journal homepage: www.sciencedirect.com

Different supported Ni catalysts for dry reforming of methane: Effect of calcination temperature

Nouf A. Bamatraf [a], Salwa B. Alreshaidan [a,*], Ahmed A. Ibrahim [b], Anis H. Fakeeha [b], Ahmed E. Abasaeed [b], Abdulaziz A.M. Abahussain [b], Mohammed F. Alotibi [c,*], Abdulaziz A. Bagabas [d], Ahmed S. Al-Fatesh [b,*]

[a] Department of Chemistry, Faculty of Science, King Saud University, P.O. Box 800, Riyadh 11451, Saudi Arabia
[b] Chemical Engineering Department, College of Engineering, King Saud University, P.O. Box 800, Riyadh 11421, Saudi Arabia
[c] Institute of Refining and Petrochemicals Technologies, King Abdulaziz City for Science and Technology (KACST), P.O. Box 6086, Riyadh 11442, Saudi Arabia
[d] Executive Office, King Abdulaziz City for Science and Technology (KACST), P.O. Box 6086, Riyadh 11442, Saudi Arabia

ARTICLE INFO

Keywords:
Metal oxide support
Ni-based catalyst
Calcination temperature
Dry reforming of methane

ABSTRACT

Due to the increased environmental consciousness about reducing greenhouse gas emissions of CH_4 and CO_2, an intriguing study issue is the dry reformation of CH_4 (DRM) over a catalyst made of Ni.). Herein in this work, 5.0 wt% NiO was loaded on various supports (S = TiO_2-P25, Al_2O_3, MgO, and ZrO_2) through the process of dry impregnation. At 600 °C or 800 °C, the catalysts were then calcined to investigate the impact of calcination temperature on the catalytic performance. The catalysts were characterized by N_2 physisorption, Raman spectroscopy, thermalgravimetric analysis, XRD, and TEM. The best catalyst was obtained when the MgO-supported Ni catalyst was operated at 700 °C and was calcined at 600 °C. This catalyst gave average conversions of CH_4 and CO_2 of 70.04 % and 77.2 %, respectively. However, when the calcination temperature of the same catalyst was increased to 800 °C, the average conversions of CH_4 and CO_2 dropped to 37.9 % and 48.07 %, respectively. Thus, the calcination pretreatment strongly influenced the catalyst performance, where rising the calcination temperature lowered the activity. The Al_2O_3-supported sample had the highest surface area, metal-support interaction, and activity. It produced a large amount of carbon nanotubes, whereas the MgO-supported sample presented the least carbon formation, the lowest deactivation factor, and no morphology change due to the reaction in the TEM.

1. Introduction

Fossil fuels account for more than 45 % of all energy in the globe. However, over the course of a century, the burning of fossil fuels has resulted in a number of issues, including the production of greenhouse gases (GHG) of CH_4 and CO_2, which are to blame for global warming and climate change (Teh et al., 2021; Ibrahim et al., 2022). To decrease the effect of these GHG, they can be transformed into high-value products like synthesis gas (syngas), which is considered a source of clean energy of hydrogen, often used in fuel cell technology (Araiza et al., 2021). Hydrogen is a benign fuel to the environment, which can be employed for powering engines, producing electricity, and many other industrial applications (Rubio and Jaojaruek, 2016; Kurdi et al., 2022). The conversion of methane into syngas can be accomplished by one of the four different reforming processes: partial oxidation of CH_4, methane decomposition, dry reforming of CH_4, or steam reforming of CH_4 (Arora and Prasad, 2016).

DRM is a highly endothermic process (Eq. (1)), which requires a high temperature (>600 °C) to complete the conversion and minimize coke formation (Al–Fatish et al., 2009).

$$CO_2 + CH_4 \rightarrow 2H_2 + 2CO \qquad \Delta H^0_{298k} = 247 \text{ kJ/mol} \tag{1}$$

$$CO_2 + H_2 \rightarrow H_2O + CO \qquad \Delta H^0_{298k} = 41 \text{ kJ/mol} \qquad \text{Reverse water gas shift} \tag{2}$$

$$CH_4 \rightarrow 2H_2 + C \qquad \Delta H^0_{298k} = 75 \text{ kJ/mol} \qquad \text{Methane decomposition} \tag{3}$$

* Corresponding authors.
E-mail address: aalfatesh@ksu.edu.sa (A.S. Al-Fatesh).

https://doi.org/10.1016/j.jksus.2023.102958
Received 18 February 2023; Received in revised form 10 August 2023; Accepted 18 October 2023
Available online 20 October 2023

Table 1
N_2 physisorption results of the catalysts obtained at two different calcination temperatures.

Sample	S_{BET} (m^2/g)	V_p (cm^3/g)	D_p (nm)
5 %Ni/TiO_2 (800 °C)	3	0.03	39.04
5 %Ni/Al_2O_3 (800 °C)	175	0.64	13.23
5 %Ni/MgO (800 °C)	37	0.35	42.32
5 %Ni/ZrO_2 (800 °C)	14	0.12	34.47
5 %Ni/TiO_2 (600 °C)	35	0.33	40.23
5 %Ni/Al_2O_3 (600 °C)	196	0.62	11.44
5 %Ni/MgO (600 °C)	55	0.52	39.77
5 %Ni/ZrO_2 (600 °C)	24	0.21	36.06

$$2CO \rightarrow CO_2 + C \qquad \Delta H^0_{298k} = -172 \text{ kJ/mol} \qquad \text{Boudouard} \tag{4}$$

However, many side reactions may occur including Eq. (2) of the reverse water gas shift (RWGS), affecting the H_2/CO mole ratio. The high reaction temperatures of DRM process facilitate the simultaneous RWGS reaction, and hence, decreases the H_2/CO mole ratio below the unity (Wang et al., 2018). Therefore, the effect of the RWGS reaction can be minimized by using lower reaction temperatures, higher mole ratios of CH_4/CO_2 in the feed of the reactants (Djinović et al., 2012), or suitable promoter (Saleh et al., 2023). Nevertheless, increasing the mole ratios of CH_4/CO_2 (>1) boosts the deactivation of the catalyst by carbon deposition via methane decomposition (Eq. (3)) or Boudouard reaction (Eq. (4)) (Bhattar et al., 2021).

For DRM reactions, there are different types of catalysts, based on either noble or non-noble metals (da Fonseca et al., 2020; Hu et al., 2022; Wu et al., 2019). Noble metals such as iridium (Ir), rhodium (Rh), ruthenium (Ru), platinum (Pt), and palladium (Pd) have higher prices and resistance to carbon deposition in comparison to non-noble metals (Lou et al., 2017; Wang et al., 2014; Zhang et al., 2021). Therefore, the usage of non-noble metals is convenient due to their prices and availability (Abdullah et al., 2017; Bian et al., 2020; Usman et al., 2015). The nickel (Ni)-based catalyst is considered the best catalyst for DRM reaction because it is highly active and economical (Rosdin et al., 2021; Wang et al., 2022a).

The calcination temperature affects the structures of the supports (Yang and Moon, 2017; Zhang et al., 2020). Researchers have performed several investigations to illustrate how this parameter affects the formulation of the catalyst (Zhang et al., 2022). High temperatures distort the carrier structure, lower the specific surface area, and sinter the active species, as opposed to low-temperature calcination, which may result in incomplete breakdown of the metal salt precursor and a corresponding reduction in the active component (Sharifianjazi et al., 2022; Wang et al., 2015). With and without calcination, the catalysts' Fischer-Tropsch activities were assessed. (Steynberg et al., 2004). It was found that for all catalysts, calcination in air improved their selectivity towards the diesel component. (Al-Fatesh, 2017; Steynberg et al., 2004). However, concentrating on the impact of calcination temperatures, Sun et al. (2019) detailed the efficiency of DRM over N_2-doped activated carbon (Co/AC-N) catalysts. Their findings showed that the calcination temperature had an effect on the catalytic activity because it changed the molar ratio of Co^{2+} to Co^{3+} and the amount of N_2 functional groups. Supported nickel catalysts are generally appealing choices for the dry reforming of CH_4, however coke deposition and Ni agglomeration prevent commercial use. Therefore, proper support should be searched (Wang et al., 2022b). In this work, oxides of TiO_2-p25, Al_2O_3, MgO, or ZrO_2 were chosen for their significant impacts on the activity and stability of the catalyst for the improvement of the process performance.

In this present study, the impact of calcination temperature (600 °C or 800 °C) on the overall catalyst efficiency in DRM was elaborated for 5.0 wt% NiO, supported on TiO_2-p25, Al_2O_3, MgO, or ZrO_2 via the dry impregnation technique.

2. Experiment

2.1. Ingredients

Hexahydrate of nickel nitrate [Ni $(NO_3)_2{\cdot}6H_2O$, 98 %, Alfa Aesar], titania (TiO_2-P25, 99.9 %, from Degussa p25, Nanoshel, Cheshire, UK), alumina (Al_2O_3, 97.7 % Norton Chemical Process Products Corp), magnesia (MgO, 99.5 %. BDH), and zirconia (ZrO_2, 99.8 %, Anhui-Elite, China) were obtained commercially and were used as received.

2.2. Catalyst preparation

The catalysts were prepared by the dry impregnation method. Accordingly, the 5.0 wt% NiO supported over S (S = TiO_2, Al_2O_3, MgO, or ZrO_2) catalysts were produced by dissolving 0.5 g of Ni $(NO_3)_2{\cdot}6H_2O$ in 30 mL of distilled water with stirring and heating. Afterwards, 2.441 g of support was added and the stirring was continued for 30 min. The obtained catalysts were dehydrated at 120 °C for 20 h and were then calcined for five hours either at 600 °C or 800 °C.

2.3. Catalyst characterization

The synthesized catalysts were characterized by using X-ray diffraction (XRD), Brunauer-Emmett-Teller (BET) nitrogen physisorption, H_2 temperature-programmed reduction (H_2-TPR),

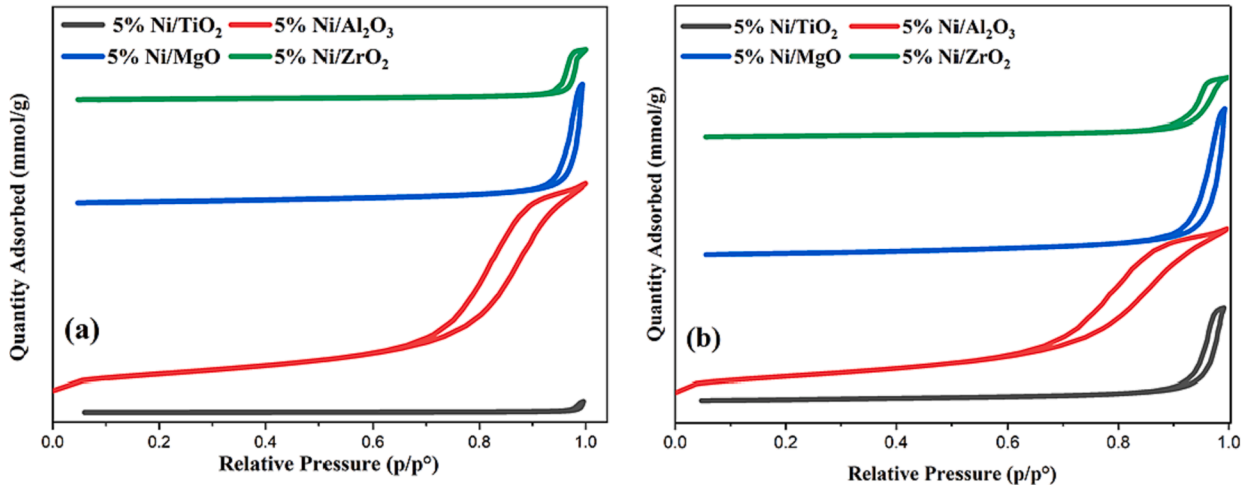

Fig. 1. N_2 adsorption–desorption isotherms for the catalysts calcined at (a) 800 °C or (b) 600 °C.

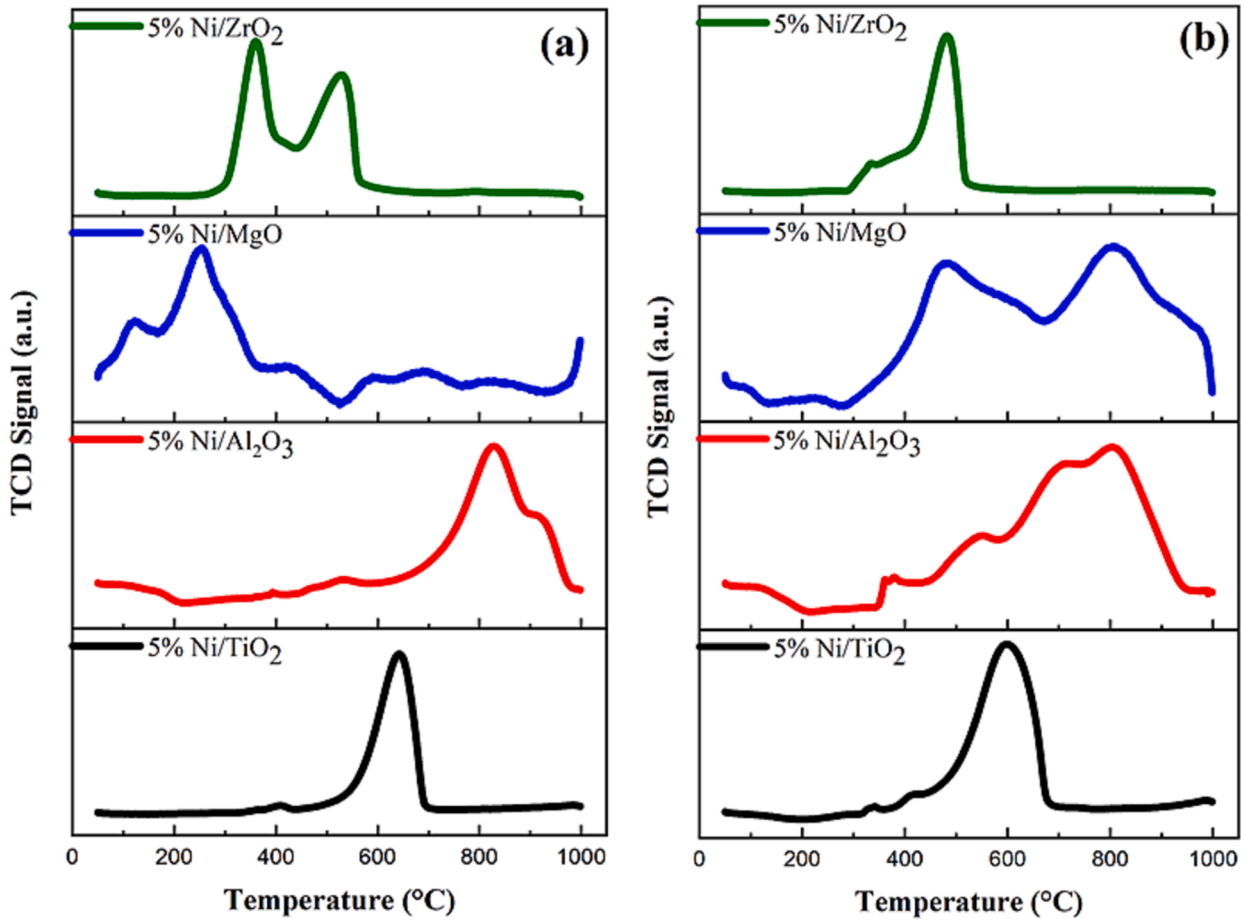

Fig. 2. H_2-TPR profiles of catalysts calcined at (a) 800 °C and (b) 600 °C.

thermogravimetric analysis (TGA), Raman spectroscopy, and transmission electron microscopy (TEM).

X-ray diffraction measurements were performed to examine the diffraction profiles of the catalysts. XRD was performed on a Rigaku (Miniflex) diffractometer, employed with Cu K_α radiation, operated at 40 kV and 40 mA. The scanning range for 2θ angle was 10–85° with a 0.02° step. X'pert high score plus software was used to analyze the raw data file. The peak intensity was measured and the ASCII file was generated at granularity 8, bending factor 5, minimum peak significance of 1.0, minimum peak width 0.40, maximum tip width 1, and peak base width 2 by minimum second derivatives. Furthermore, different phases with their scores were matched with the JCPDS data bank and X'pert high score plus software.

The Micromeritics Auto Chem II device was used to carry out the H_2-TPR assessments. For H_2-TPR, a catalyst sample weighing 70 mg was pre-treated with a stream of high purity Argon (Ar) at 150 °C for 30 min before being cooled to 25 °C. The sample was then heated in an automated furnace at atmospheric pressure to 1000 °C at a constant heating rate of 10 °C/min while flowing at a rate of 40 mL/min of an H_2/Ar mixture. (volume ratio, 10/90). The signal of H_2 consumption was monitored by a thermal conductivity detector (TCD).

Using data from N_2 adsorption–desorption at 196 °C, the BET-specific surface areas of the fresh catalysts were calculated using a Micromeritics Tristar II 3020 surface area and porosity analyzer. About 0.2–0.3 g of catalyst were employed for each study. Before the measurement, the samples were degassed at 250 °C for 180 min to eliminate the moisture content and other gases that had been adsorbed to the catalysts' surface. Through the use of the Barrett, Joyner, and Halenda (BJH) approach, the pore distribution was determined from the adsorption branch of the associated N_2 isotherm.

The quantitative analysis of coke deposition on the surface of the spent catalysts, after six-hour reaction at 700 °C, was carried out by TGA under air atmosphere by using a Shimadzu Thermogravimetric/Differential analyzer. A sample of around 15 mg of the used catalyst was heated till 1000 °C at a rate of 20 °C/min., and the weight loss was calculated. On a JASCO NRS-4500 laser Raman spectrometer, the used catalysts' Raman spectra were captured in the spectral region between 1400 and 1600 cm^{-1}. Using an objective lens with a 100X magnification, the excitation beam's wavelength was set to 532 nm. To avoid sample damage from laser irradiation, the laser power was adjusted to 1.6 mW for 10 s of exposure time at three accumulations. The spectra were processed using the Spectra Manager Ver.2 program (JASCO, Japan). The TEM-1011 is a high-performance, high-contrast 100 kV TEM with excellent imaging, an easy-to-use instrument with an acceleration voltage of 40–100 kV. TEM has been used in all areas of biological and biomedical investigations (HRTEM model: JEOL 1011, Japan).

2.4. Catalytic activity test

In a fixed-bed, continuous-flow reactor (PID Eng. & Tech), the catalytic activity was assessed for 7 h. The dry reforming reaction was carried out over a sample of 0.1 g of catalyst, at atmospheric pressure, in a 0.94 cm internal diameter and 30 cm long stainless-steel tube. A thermocouple that was positioned in the center of the catalyst bed was used to regulate and monitor the temperature of the reactor. Before the response, hydrogen (H_2) was introduced, at a flow rate of 40 mL/min, at 800 °C to convert nickel oxide to nickel metal, the active form of the catalyst. Afterward, the reactor was purged under nitrogen (N_2) flow (20 mL/min) to remove any H_2 left in the reactor. Then the reactor

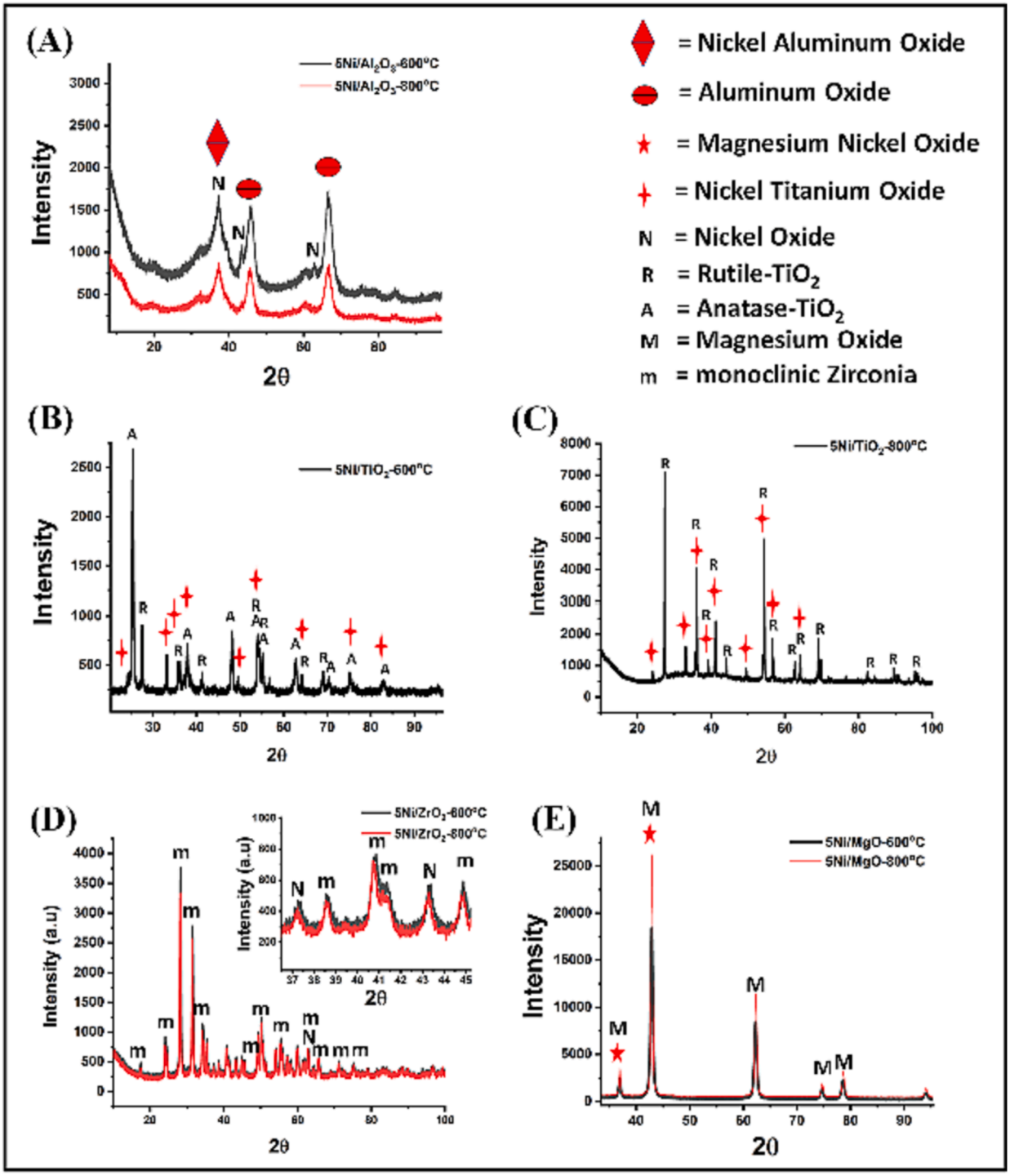

Fig. 3. XRD patterns of Ni/S catalysts (S = TiO_2, Al_2O_3, MgO or ZrO_2).

temperature was adjusted, under the flow of N_2 until the reaction temperature of 700 °C was reached. A total feed flow rate of 70 mL/min, consisting of 27.5, 27.5, and 15 mL/min of CH_4, CO_2, and N_2, respectively. The space velocity was set at 42,000 mL$(h.g_{cat})^{-1}$. Online gas chromatography using a TCD was used to analyze the reactor exit gases, which contained syngas and unconverted feed gases. For the total separation of reaction products, Porapak Q and Molecular Sieve 5A, were employed in series/bypass connections. (M. Zhang et al., 2020). The following formulas were used in this work to compute the conversions of CH_4 and CO_2 in addition to the H_2/CO mole ratio:

$$\%CH_4 \text{ conversion} = \frac{\text{mole of } CH_4 \text{ in} - \text{mole of } CH_4 \text{ out}}{\text{mole of } CH_4 \text{ in}} \times 100$$

$$\%CO_2 \text{ conversion} = \frac{\text{mole of } CO_2 \text{ in} - \text{mole of } CO_2 \text{ out}}{\text{mole of } CO_2 \text{ in}} \times 100$$

$$H_2 \text{ and CO ratio} = \frac{\text{moles of } H_2 \text{ produced}}{\text{moles of CO produced}}$$

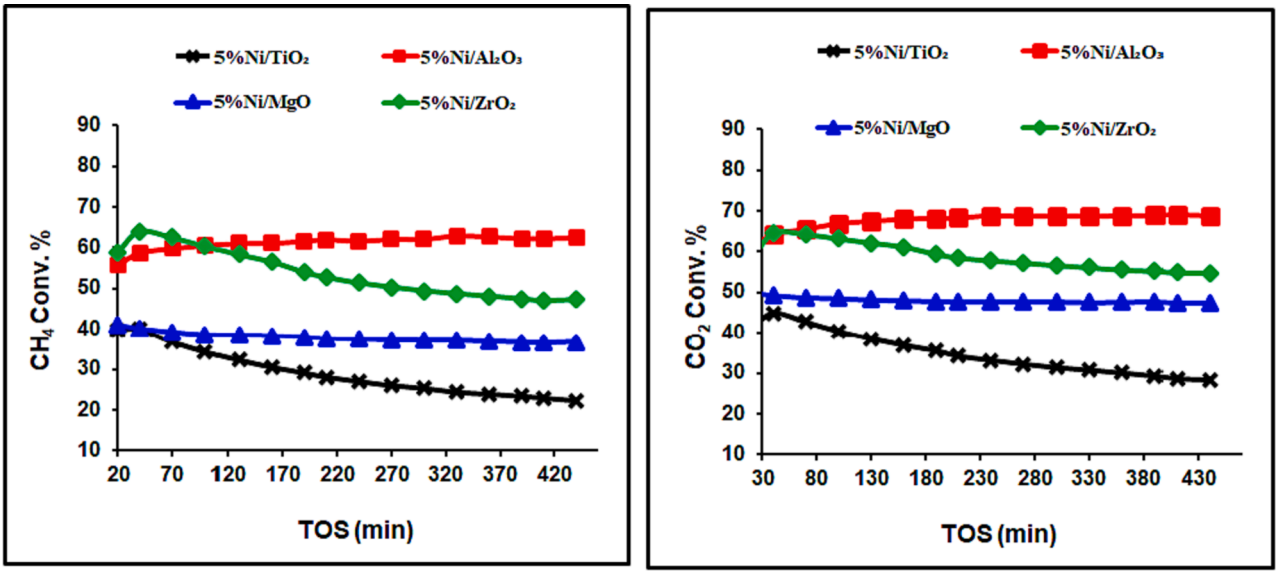

Fig. 4. CH_4 and CO_2 conversions over catalysts, calcined at 800 °C.

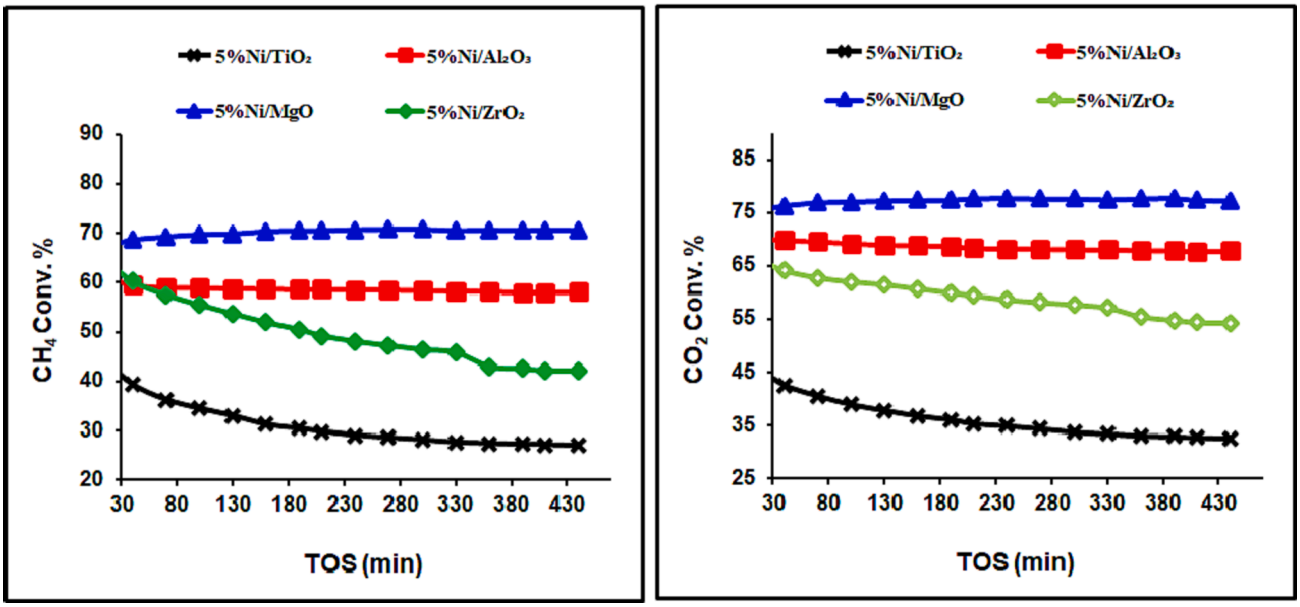

Fig. 5. CH_4 and CO_2 conversions over catalysts, calcined at 600 °C.

3. Results and discussion

3.1. Characterization results

3.1.1. BET (Brunauer-Emmett-Teller) analysis

The surface area, average pore diameter, and pore volume for all catalysts are summarized in Table 1. From the surface area of catalysts, increasing calcination temperature decreased surface area. Fig. 1 shows N_2 adsorption–desorption isotherms of the catalysts, obtained at two different calcination temperatures. The catalysts showed type-IV isotherms with an H1-type hysteresis loop according to the IUPAC classification, describing a mesoporous structure (Sing, 1985).

3.1.2. H_2-TPR

Temperature-programmed reduction (TPR) is a technique used to study the reducibility of catalysts. The TPR profile of a catalyst can provide information about the different types of metal oxides present on the catalyst surface, as well as their reducibility. Because of their high activity and low cost, nickel- and cobalt-based catalysts have been widely studied for DRM; however, their poor stability due to coke production has prevented their commercialization. Few papers have concentrated on the advantages of bimetallic catalysts for reducing coke formation, despite the fact that many have addressed the many features of catalyst deactivation and mitigation measures. Due to the synergistic effects brought about by two metal-to-metal contacts, bimetallic catalysts frequently exhibit greater catalytic stability than their monometallic counterparts (Sasson Bitters et al., 2022). Liu et al. (2022) used a series of confined indium-nickel (In-Ni) intermetallic alloy nanocatalysts ($InxNi@SiO_2$) and showed superior coking resistance for DRM reaction. Here, the Ni metal is the active site of the Ni/S catalysts (S = TiO_2, Al_2O_3, MgO, or ZrO_2). The reducibility was determined, as exhibited in Fig. 2. For the catalysts calcined at 800 °C, the MgO-supported Ni catalyst did not show any reduction peak beyond 300 °C. This observation indicated the catalyst's structure was deformed and

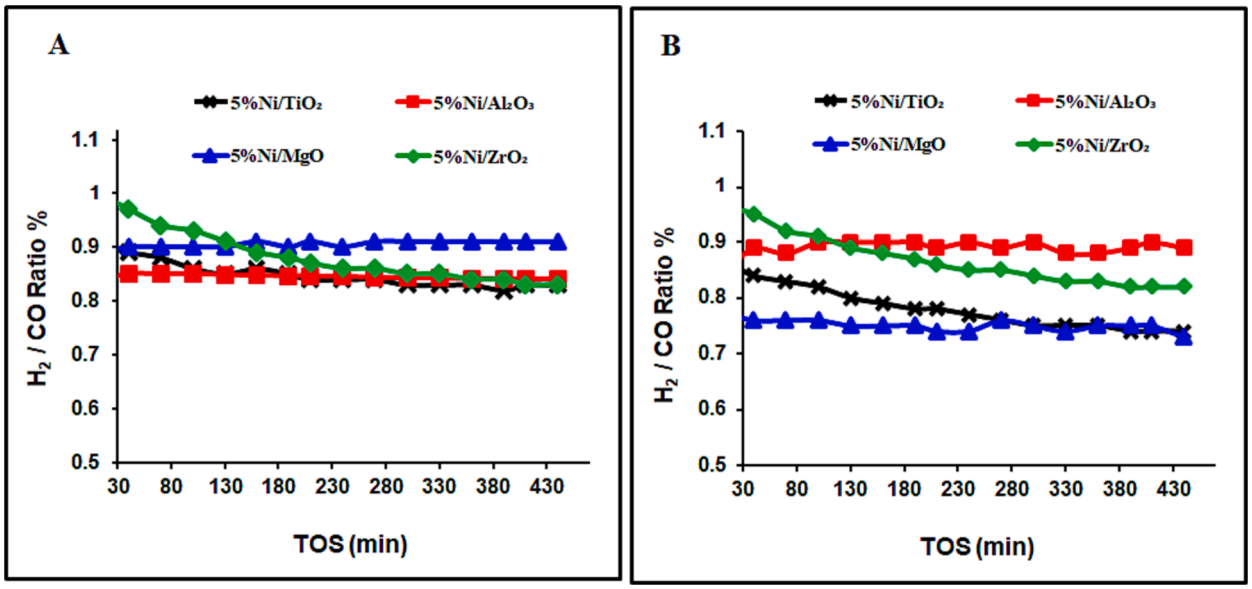

Fig. 6. H_2/CO ratios over catalysts, calcined at (a) 800 °C and (b) 600 °C.

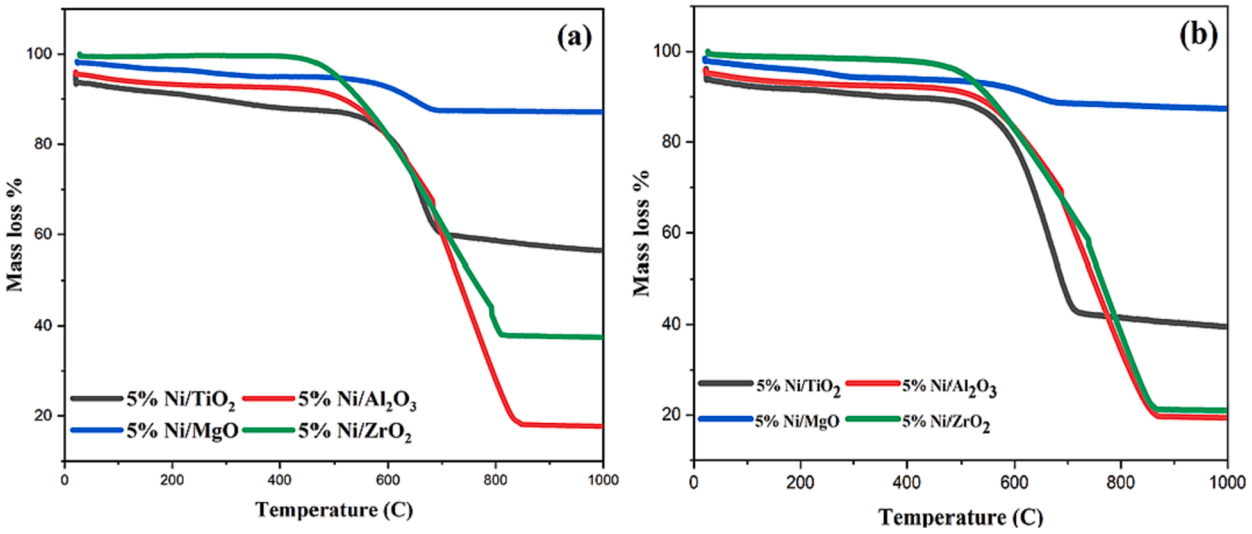

Fig. 7. TGA curves of catalysts calcined at (a) 800 °C and (b) 600 °C.

Table 2
Examination of catalyst performance.

Sample	Calcination temperature (°C)	Conversion				Carbon deposits (%)	Deact. Factor (DF) (%)
		CH_4		CO_2			
		Initial	Final	Initial	Final		
Ni/ TiO_2	800 °C	39.79	22.26	41.27	28.32	39	44
Ni/Al_2O_3	800 °C	55.71	62.40	60.95	68.84	78.29	12
Ni/MgO	800 °C	41.01	36.69	50.04	47.39	11.19	10
Ni/ZrO_2	800 °C	58.84	46.98	58.05	54.91	62.55	20
Ni/ TiO_2	600 °C	43.33	27.65	45.36	33.40	56.7	36
Ni/Al_2O_3	600 °C	61.00	58.10	70.00	67.85	76.48	4.75
Ni/MgO	600 °C	67.50	70.5	75.42	77.20	11.03	4.4
Ni/ZrO_2	600 °C	63.88	42.19	65.95	54.36	78.97	33

Coke = acquired from TGA after 7-hour reaction; % DF = ABS (CH_4 conversion at the beginning- CH_4 conversion at the end)/ CH_4 conversion at the beginning × 100; Beginning = 20 min; End = 440 min.

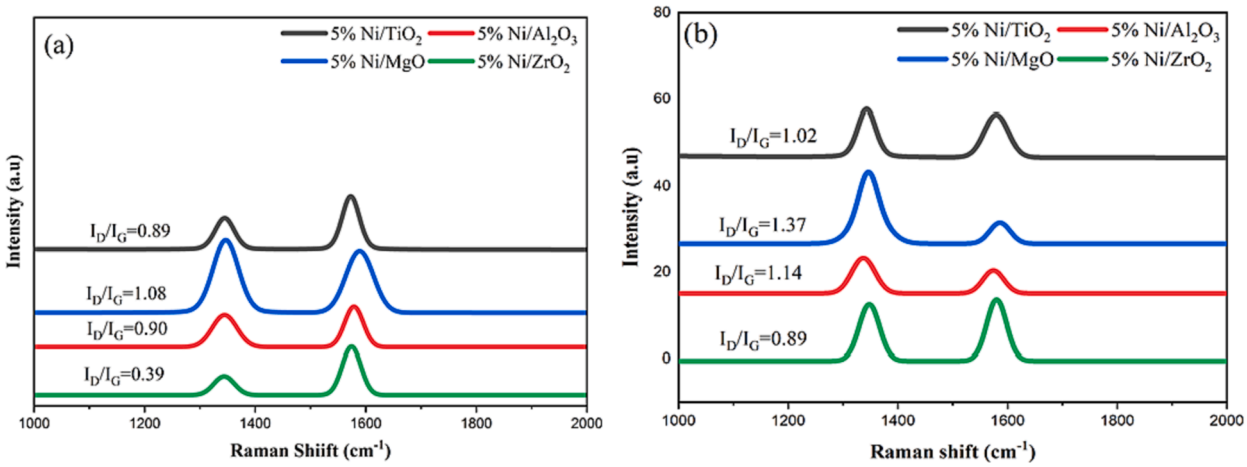

Fig. 8. Raman spectra of the used samples, calcined at (a) 800 °C and (b) 600 °C.

there was no reducible NiO on the calcined surface owing to the strong interaction of NiO with MgO support and the formation of solid-state solution (Bagabas et al., 2021). The TiO_2-supported catalyst exhibited a single peak at 600 °C, indicating a modest interaction between the support and the NiO. On the other hand, the Al_2O_3-supported Ni catalyst gave a peak at 800 °C, showing a strong interaction due to the formation of $NiAl_2O_4$ spinel. The ZrO_2-supported catalyst displayed two peaks at 320 °C and 500 °C, ascribable to weak and moderate interactions. For catalysts calcined at 600 °C, the Ni supported over MgO gave broad peaks at around 450 °C and 800 °C, which could be related to moderate and very strong interactions. The Al_2O_3-supported Ni catalyst gave a broad peak at around 830 °C, indicating the formation of $NiAl_2O_4$ spinel compound. The TiO_2-supported Ni catalyst gave a peak at 600 °C for moderate interaction, while ZrO_2-supported sample displayed a peak at 480 °C with a shoulder at 320 °C for moderate interaction.

3.1.3. XRD analysis

As exhibited in Fig. 3, the fresh catalysts' crystallinity and structural details were ascertained using X-ray diffraction analysis. The cubic phase of nickel aluminum oxide may be responsible for the diffraction peaks at 37.30° and 45.48°. (Ref. Code 00-001-1299); at 43.27° and 62.86° might be related to the cubic phase of NiO (Ref. code 01-071-1179); and at 37.30°, at 46.02° and 66.55° might be linked to aluminum oxide's cubic phase (Ref. Code 00-001-1299), as shown in Fig. 3(A). In Fig. 3(B–C), we observed the rhombohedral nickel titanium oxide phase (Ref. Code 01-076-0334) at 24.2°, 33.17°, 35.7°, 38.69°, 40.97°, 49.5°, and 54.03°; anatase phase (Ref. Code 00–021-1272) at 25.37°, 37°, 37.9°, 38.69°, 48.12°, 54.03°, 55.19°, 62.80°, 70.44°; and 75.09°; and rutile phase (Ref. Code 01–078-1510; 01–076-0334) at 27.5°, 36.19°, 41.37°, 54.39°, 56.71°, 62.80°, 64.15°, 69.08°, 76.53°, 82.35°, 84.27°, and 89.54°. In Fig. 3(D), we detected the cubic phase of NiO (Ref. Code 01-075-0269) at 37.33°, 43.31°, and 62.84°; and the monoclinic phase of zirconium oxide (Ref. Code 00-024-1165) at 17.52°, 24.10°, 24.52°, 28.25°, 31.52°, 34.17°, 34.52°,35.39°, 40.78°, 41.43°, 44.88°, 45.66°, 49.27°, 50.13°, 50.67°, 54.11°, 55.50°, 56.06°, 57.18°, 59.9°, 62.84°, 65.74°, and 71.27°. In Fig. 3(E), we found the cubic phase of magnesium nickel oxide (Ref. Code: 00-034-0410) at 36.92°, and 42.93°; and the cubic phase of magnesium oxide (Ref. Code: 00-043-1022) at 36.92°, 42.93°; 62.33°, 74.61°, 78.53°, and 93.93°. Thus, XRD analysis exhibited all the expected phases due to NiO, the support, and the way NiO interacts with the support in our prepared catalysts.

3.2. Catalyst activity results

Ni-based catalysts are common for endothermic reactions, where the major hindrance to their industrial application is the salient coke deposition, causing their deactivation. Therefore, CO_2 reforming of methane needs the employment of stable, effective catalysts, resistant to coking with the focus on the metal activity, the kind of support, and the operation conditions.

Preliminary experiments were performed to evaluate the behavior of our prepared catalysts as a function of reaction time. The obtained results are shown in Fig. 4. The CO_2 conversion of all catalysts was somewhat higher than that of CH_4, which was regularly attributed to the presence of the reverse water gas shift reaction, as per Eq. (2) (Sun et al., 2019).

Figs. 4 and 5 reveal the average carbon dioxide and methane conversions were higher for the catalysts, calcined at 600 °C than those, calcined at 800 °C, irrespective of support identity. The 5 %Ni/Al_2O_3 Catalyst with the highest activity could be assigned to its highest specific surface area and the strongest NiO contact with the support, which prevents metallic Ni from sintering. On the other hand, the selectivity of the DRM catalysts is expressed in term of the H_2/CO ratio, as seen in Fig. 6. This parameter is linked to the efficiency of the catalysts to suppress side reactions like coking and the reverse water gas shift reactions. Increasing calcination temperature helped the RWGS reaction and increased the CO_2 conversion, which consumed H_2 and lowered the DRM efficiency.

3.2.1. TGA of the spent samples

As seen in Fig. 7, the weight loss began at about 500–550 °C due to the elimination of various carbon species. Amount of carbon that has been deposited on Ni/S catalysts (S = TiO_2, Al_2O_3, MgO, or ZrO_2) and their corresponding deactivation factors were given in Table 2, indicating that the temperature's impact on calcination on both support identity and amount of deposited carbon. The Al_2O_3-supported catalysts gave the highest carbon deposition regardless of calcination temperature. Moreover, the MgO-supported catalysts generated the least carbon formation and deactivation factors. The least active TiO_2-supported catalyst assumed the highest deactivation factors. The ZrO_2-supported catalysts generated sufficient carbon formation and deactivation factors. In general, the deactivation factor decreases with the calcination temperature. The alumina-supported catalyst presented the highest carbon formation as shown by the TGA analysis. The same catalyst displayed the highest metal-support interaction and the highest activity.

The catalytic activity results vis-à-vis carbon deposit formation over Ni/TiO_2, Ni/Al_2O_3, Ni/MgO, and Ni/ZrO_2 catalysts are needed to be discussed. Irrespective of calcination temperature, 5 %Ni/Al_2O_3 has an adequate amount of reducible NiO-species having strong metal support interaction about DRM temperature (800 °C). The catalyst gives ~ 60 % CH_4 conversion with ~77 % carbon deposit. The huge carbon deposit doesn't seem to affect the activity due to proper matching of the rate of

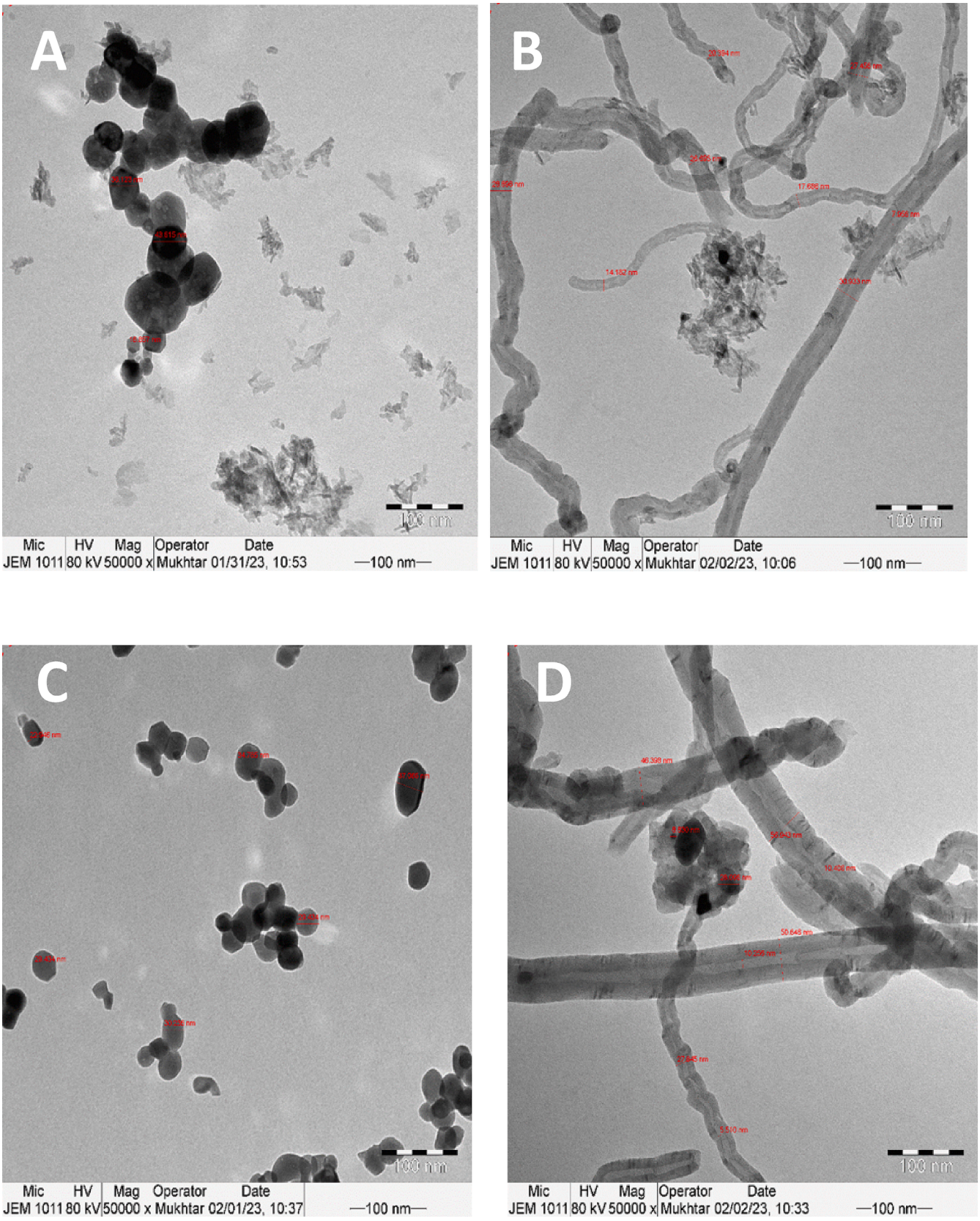

Fig. 9. TEM images of catalysts supported on alumina (A) fresh and (B) spent; zirconia (C) fresh and (D) spent; titania (E) fresh and (F) spent; and magnesia (G) fresh and (H) spent.

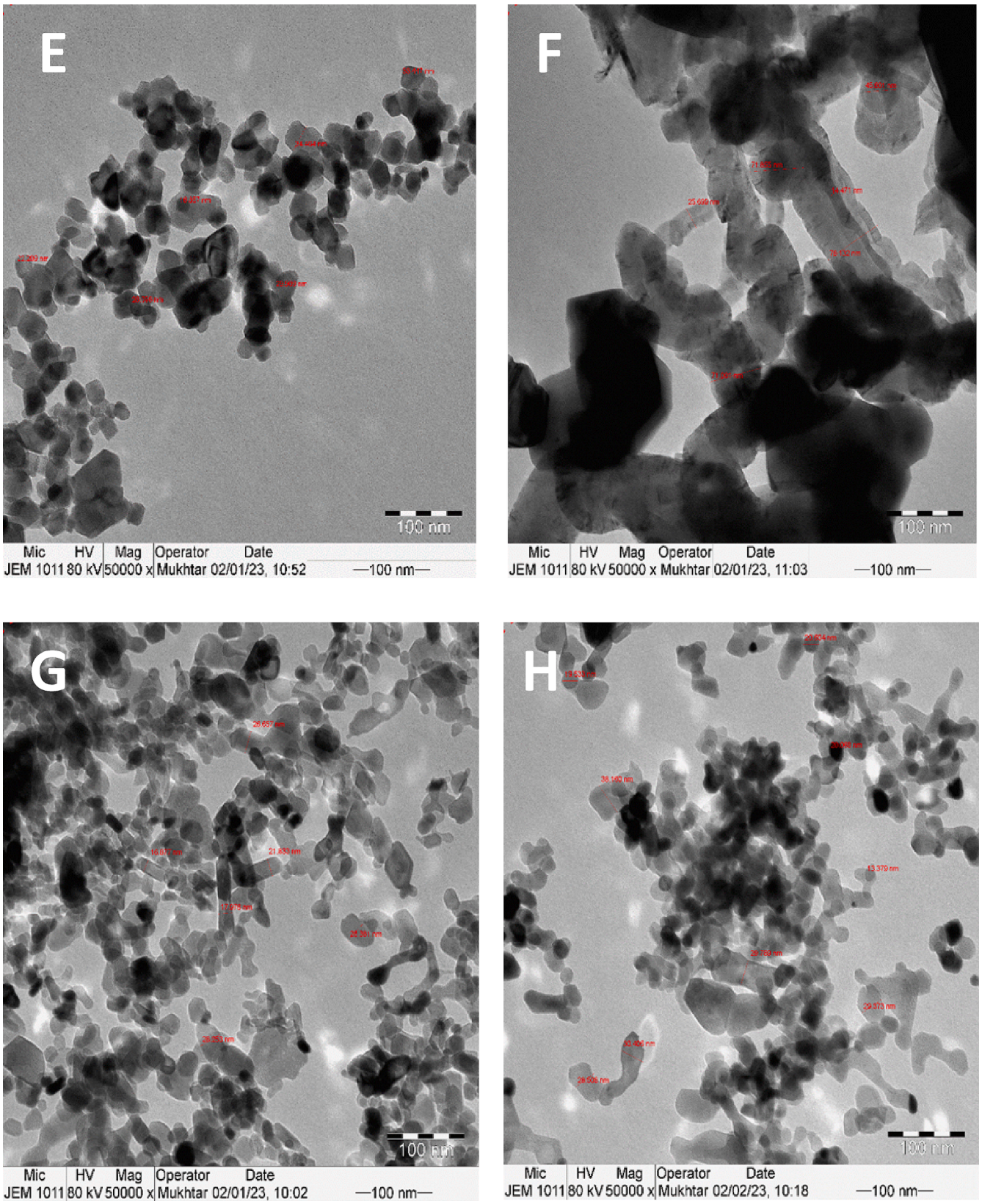

Fig. 9. (*continued*).

carbon formation (at the catalytic active site) with carbon diffusion rate (away from active sites) (Bayahia et al., 2023). Ni/MgO calcined at lower temperature has relatively lower crystallinity and reducible NiO is present, and it has a moderate to strong interaction with support. Ni/MgO calcined at higher temperatures is highly crystalline and it has lack strong metal-support interaction. So, the previous one has double the CH_4 conversion than the latter. However, Ni/MgO has excellent coke resistance properties as it retains a minimum coke deposit (~11 %). That

means, whatever amount of CH_4 is decomposed over metallic Ni (at Ni/MgO catalyst), those are mostly oxidized by CO_2. The phase distribution over Ni/ZrO_2 and Ni/TiO_2 is not affected by calcination temperature and both catalysts lack strong metal-support interaction. On comparing the reducibility profile of both catalysts, it is found that the reducibility pattern of Ni/ZrO_2 is shifted to a relatively lower temperature which indicates the easier reducibility of NiO over Ni/ZrO_2 catalyst than over Ni/TiO_2 catalyst. It renders higher CH_4 decomposition as well as carbon deposit accumulation over Ni/ZrO_2 than Ni/TiO_2.

3.2.2. Raman analysis

Additional information regarding the degree of graphitization and the type of deposited carbon on the used catalysts is provided by the Raman spectra (Fig. 8). Zones can be divided up into the spectra. Zones I and II are respectively located between 1250 and 1650 cm^{-1} and 2400 and 2800 cm^{-1}, in the order given. The D-band and G-band's main characteristic peaks in zone I were located at 1346 cm^{-1} and 1571 cm^{-1}, respectively. Amorphous (disordered) carbon deposits were identified by the D-band, while graphite was identified by the G-band. The 2D band is visible at 2666 cm^{-1} due to the band of zone I's unification and ramifications. The amount of carbon crystallinity produced during the reaction was calculated using the relative intensities of the G and D bands (ID/IG), where the small ratios specified the dominance of crystallinity due to the graphitized carbon. The ID/IG measurements for the investigated catalysts were 1.02, 1.14, 1.37, and 0.89 for the 5 %Ni/TiO_2, 5 %Ni/Al_2O_3, 5 %Ni/MgO and 5 %Ni/ZrO_2, respectively, for the samples calcined at 600 °C. The highest (ID/IG) ratios were seen in the Ni/MgO catalysts, showing low carbon crystallinity as a result of a lack of graphitized carbon. As a result, the 5 %Ni/MgO catalyst's carbon crystallinity was less prominent than that of other catalysts, and its degree of graphitization was clearly reduced. Similar spectra were obtained if the calcination temperature is increased to 800 °C. However, the ratios of the intensities dropped indicating the increase in crystallinity and the carbon graphitization.

3.2.3. TEM

Fig. 9 depicts the TEM pictures of the spent Ni/S catalysts (S = TiO_2, Al_2O_3, MgO, or ZrO_2), calcined at 600 °C before DRM reaction, at 100 nm scale. Fig. 9A and B are for the fresh and spent alumina-supported catalysts, where the agglomerated catalyst particles were observed for the fresh, while carbon nanotubes of different sizes were detected in the spent sample. Similarly, Fig. 9C and D are for the fresh and spent zirconia-supported samples. The used catalyst demonstrated the development of carbon filamentous nanotubes, while the fresh sample showed scattered groups of agglomerated particles. Fig. 9E and F are for the fresh and spent titania-supported samples. The fresh sample displayed a string of attached particles, while the spent showed large size carbon nanotubes, which often block the DRM reaction. On the other hand, Fig. 9G and H are for the fresh and spent magnesia-supported samples. The fresh and the spent samples resembled each other, indicating the absence of filamentous carbon formation. The TEM of the used alumina-supported showed the distinct carbon nanotube formation in accordance with TGA analysis where the largest carbon deposition occurred. On the other hand, the MgO-supported sample with the least carbon deposition in TGA analysis exhibited no variation morphology of the used TEM image.

3.3. Process performance

For the present work, the dry reforming of CH_4 employing Ni/MgO sample which was calcined at 600 °C and then worked at 700 °C for 7 h produced CH_4 and CO_2 conversions of 70 % and 77 % respectively. While (Qiu et al., 2022); studied the DRM at 700 °C and 1 atmosphere for 2 h using Ni/ Al_2 O_3 catalysts. Their results displayed CH_4 and CO_2 conversions of 63.8 % and 74 % respectively. Alternatively Rosdin et al. (2021); investigated the dry reforming of methane at 650 °C and 1 atmosphere for 5 h using Ni/Al_2O_3 catalysts. The support is modified by doping it with ZrO_2 and MgO. Their results exhibited efficient CH_4 and CO_2 conversions of 27 and 39 % respectively using Ni/Al_2O_3-MgO catalyst. On the other hand, Ibrahim et al. (2022) examined the DRM at 700 °C for various calcination temperatures using Ni/ZrO_2. When 600 °C calcination was used the CH_4 and CO_2 conversions of 46 % and 62 % respectively were obtained for a 7 h reaction. While 800 °C calcination generated CH_4 and CO_2 conversions of 76 % and 60 % respectively for 4.6 h.

4. Conclusions

The goal of the current work was to create 5.0 % NiO/S by the dry impregnation technique for DRM. Two different calcination temperatures were used for investigating the impact of this parameter on the catalyst activity. Specific surface area values between 3 and 195 m^2/g were identified by the N_2-physisorption, and it was shown that lower calcination temperatures often resulted in higher surface areas. The catalyst with 5 % Ni/Al_2O_3 had the biggest surface area, the best activity performance against DRM, and the lowest 5 % deactivation factor after being calcined at 600 °C. On the other hand, the 5 %Ni/MgO and 5 %Ni/TiO_2 catalysts displayed the lowest carbon deposition, as reflected by their corresponding weight loss of 11.11 % and 47.85 %, respectively. The amount of crystallinity of the carbon generated during the DRM reaction was measured using the Raman bands of the used samples. Compared to other catalysts, the Ni/MgO had a lower crystallinity and a noticeably lower degree of graphitization. The support, the predicted phases of NiO, and the interplay of NiO with the support were all visible in the XRD images of the new catalysts. Since the surface area and activity of the catalyst reduced as the calcination temperature rose, the calcination pretreatment had an impact on how well the catalyst performed. The best catalyst supported by alumina displayed the highest strength interaction between the NiO and the support.

Declaration of Competing Interest

The authors declare that they have no known competing financial interests or personal relationships that could have appeared to influence the work reported in this paper.

Acknowledgments

The writers want to express their sincere gratitude to Researchers Supporting Project number (RSP2023R368), King Saud University, Riyadh, Saudi Arabia.

References

Abdullah, B., Abd Ghani, N.A., Vo, D.-V.-N., 2017. Recent advances in dry reforming of methane over Ni-based catalysts. J. Clean. Prod. 162, 170–185. https://doi.org/10.1016/j.jclepro.2017.05.176.

Al-Fatesh, A.S., 2017. Promotional effect of Gd over Ni/Y2O3 catalyst used in dry reforming of CH4 for H2 production. Int. J. Hydrogen Energy 42 (30), 18805–18816. https://doi.org/10.1016/j.ijhydene.2017.06.165.

Al–Fatish, A.S.A., Ibrahim, A.A., Fakeeha, A.H., Soliman, M.A., Siddiqui, M.R.H., Abasaeed, A.E., 2009. Coke formation during CO2 reforming of CH4 over alumina-supported nickel catalysts. Appl. Catal. A 364 (1-2), 150–155.

Araiza, D.G., Arcos, D.G., Gómez-Cortés, A., Díaz, G., 2021. Dry reforming of methane over Pt-Ni/CeO2 catalysts: Effect of the metal composition on the stability. Catal. Today 360, 46–54. https://doi.org/10.1016/j.cattod.2019.06.018.

Arora, S., Prasad, R., 2016. An overview on dry reforming of methane: strategies to reduce carbonaceous deactivation of catalysts. RSC Adv. 6 (110), 108668–108688. https://doi.org/10.1039/C6RA20450C.

Bagabas, A., Al-Fatesh, A.S., Kasim, S.O., Arasheed, R., Ibrahim, A.A., Ashamari, R., Anojaidi, K., Fakeeha, A.H., Abu-Dahrieh, J.K., Abasaeed, A.E., 2021. Optimizing MgO Content for Boosting γ-Al2O3-Supported Ni Catalyst in Dry Reforming of Methane. Catalysts 11 (10), 1233. https://doi.org/10.3390/catal11101233.

Bayahia, H., Fakeeha, A.H., Al-Zahrani, S.A., Alreshaidan, S.B., Al-Awadi, A.S., Alotibi, M.F., Kumar, R., Al-Fatesh, A.S., 2023. COx -free H2 Production via Catalytic Decomposition of CH4 over Fe Supported on Tungsten oxide-activated Carbon

Catalyst: Effect of Tungsten Loading. Arab. J. Chem. 16 (6), 104781 https://doi.org/10.1016/j.arabjc.2023.104781.
Bhattar, S., Abedin, M.A., Kanitkar, S., Spivey, J.J., 2021. A review on dry reforming of methane over perovskite derived catalysts. Catal. Today 365, 2–23. https://doi.org/10.1016/j.cattod.2020.10.041.
Bian, Z., Wang, Z., Jiang, B., Hongmanorom, P., Zhong, W., Kawi, S., 2020. A review on perovskite catalysts for reforming of methane to hydrogen production. Renew. Sustain. Energy Rev. 134, 110291 https://doi.org/10.1016/j.rser.2020.110291.
da Fonseca, R.O., Rabelo-Neto, R.C., Simões, R.C.C., Mattos, L.V., Noronha, F.B., 2020. Pt supported on doped CeO2/Al2O3 as catalyst for dry reforming of methane. Int. J. Hydrogen Energy 45 (8), 5182–5191. https://doi.org/10.1016/j.ijhydene.2019.09.207.
Djinović, P., Osojnik Črnivec, I.G., Erjavec, B., Pintar, A., 2012. Influence of active metal loading and oxygen mobility on coke-free dry reforming of Ni–Co bimetallic catalysts. Appl. Catal. B 125, 259–270. https://doi.org/10.1016/j.apcatb.2012.05.049.
Hu, H., Ding, W., Sun, G., Yao, Z., 2022. Novel highly active and stable alumina-supported cobalt nitride catalyst for dry reforming of methane. Appl. Surf. Sci. 606, 154802 https://doi.org/10.1016/j.apsusc.2022.154802.
Ibrahim, A.A., Fakeeha, A.H., Lanre, M.S., Al-Awadi, A.S., Alreshaidan, S.B., Albaqmaa, Y.A., Adil, S.F., Al-Zahrani, A.A., Abasaeed, A.E., Al-Fatesh, A.S., 2022. The Effect of Calcination Temperature on Various Sources of ZrO2 Supported Ni Catalyst for Dry Reforming of Methane. Catalysts 12 (4), 361. https://doi.org/10.3390/catal12040361.
Kurdi, A.N., Ibrahim, A.A., Al-Fatesh, A.S., Alquraini, A.A., Abasaeed, A.E., Fakeeha, A.H., 2022. Hydrogen production from CO_2 reforming of methane using zirconia supported nickel catalyst. RSC Adv. 12 (17), 10846–10854. https://doi.org/10.1039/D2RA00789D.
Liu, W., Li, L., Lin, S., Luo, Y., Bao, Z., Mao, Y., Li, K., Wu, D., Peng, H., 2022. Confined Ni-In intermetallic alloy nanocatalyst with excellent coking resistance for methane dry reforming. Journal of Energy Chemistry 65, 34–47. https://doi.org/10.1016/j.jechem.2021.05.017.
Lou, Y., Steib, M., Zhang, Q., Tiefenbacher, K., Horváth, A., Jentys, A., Liu, Y., Lercher, J. A., 2017. Design of stable Ni/ZrO2 catalysts for dry reforming of methane. J. Catal. 356, 147–156. https://doi.org/10.1016/j.jcat.2017.10.009.
Qiu, H., Ran, J., Huang, X., Ou, Z., Niu, J., 2022. Unrevealing the influence that preparation and reaction parameters have on Ni/Al2O3 catalysts for dry reforming of methane. Int. J. Hydrogen Energy 47 (80), 34066–34074. https://doi.org/10.1016/j.ijhydene.2022.08.014.
Rosdin, R.D.B., Yusuf, M., Abdullah, B., 2021. Dry reforming of methane over Ni-based catalysts: Effect of ZrO2 and MgO addition as support. Mater. Lett.: X 12, 100095. https://doi.org/10.1016/j.mlblux.2021.100095.
Rubio, M.G.A., Jaojaruek, K., 2016. Small-scale shaking single-stage downdraft biomass gasifier. In: 2016 International Conference on Cogeneration, Small Power Plants and District Energy (ICUE), pp. 1–5. https://doi.org/10.1109/COGEN.2016.7728949.
Saleh, J., Al-Fatesh, A.S., Ibrahim, A.A., Frusteri, F., Abasaeed, A.E., Fakeeha, A.H., Albaqi, F., Anojaidi, K., Alreshaidan, S.B., Albinali, I., Al-Rabiah, A.A., Bagabas, A., 2023. Stability and Activity of Rhodium Promoted Nickel-Based Catalysts in Dry Reforming of Methane. Nanomaterials 13 (3), 547. https://doi.org/10.3390/nano13030547.
Sasson Bitters, J., He, T., Nestler, E., Senanayake, S.D., Chen, J.G., Zhang, C., 2022. Utilizing bimetallic catalysts to mitigate coke formation in dry reforming of methane. J. Energy Chem. 68, 124–142. https://doi.org/10.1016/j.jechem.2021.11.041.
Sharifianjazi, F., Esmaeilkhanian, A., Bazli, L., Eskandarinezhad, S., Khaksar, S., Shafiee, P., Yusuf, M., Abdullah, B., Salahshour, P., Sadeghi, F., 2022. A review on recent advances in dry reforming of methane over Ni- and Co-based nanocatalysts. Int. J. Hydrogen Energy 47 (100), 42213–42233. https://doi.org/10.1016/j.ijhydene.2021.11.172.
Sing, K.S.W., 1985. Reporting physisorption data for gas/solid systems with special reference to the determination of surface area and porosity (Recommendations 1984). Pure Appl. Chem. 57 (4), 603–619. https://doi.org/10.1351/pac198557040603.
Steynberg, A.P., Dry, M.E., Davis, B.H., Breman, B.B., 2004. Fischer–Tropsch Reactors (pp. 64–195). https://doi.org/10.1016/S0167-2991(04)80459-2.
Sun, Y., Zhang, G., Xu, Y., Zhang, R., 2019. Catalytic performance of dioxide reforming of methane over Co/AC-N catalysts: Effect of nitrogen doping content and calcination temperature. Int. J. Hydrogen Energy 44 (31), 16424–16435. https://doi.org/10.1016/j.ijhydene.2019.04.250.
Teh, L.P., Setiabudi, H.D., Timmiati, S.N., Aziz, M.A.A., Annuar, N.H.R., Ruslan, N.N., 2021. Recent progress in ceria-based catalysts for the dry reforming of methane: A review. Chem. Eng. Sci. 242, 116606 https://doi.org/10.1016/j.ces.2021.116606.
Usman, M., Wan Daud, W.M.A., Abbas, H.F., 2015. Dry reforming of methane: Influence of process parameters—A review. Renew. Sustain. Energy Rev. 45, 710–744. https://doi.org/10.1016/j.rser.2015.02.026.
Wang, Z., Cao, X.-M., Zhu, J., Hu, P., 2014. Activity and coke formation of nickel and nickel carbide in dry reforming: A deactivation scheme from density functional theory. J. Catal. 311, 469–480. https://doi.org/10.1016/j.jcat.2013.12.015.
Wang, J., Dong, X., Wang, Y., Li, Y., 2015. Effect of the calcination temperature on the performance of a CeMoOx catalyst in the selective catalytic reduction of NOx with ammonia. Catal. Today 245, 10–15. https://doi.org/10.1016/j.cattod.2014.07.035.
Wang, Y., Li, L., Cui, C., Da Costa, P., Hu, C., 2022a. The effect of adsorbed oxygen species on carbon-resistance of Ni-Zr catalyst modified by Al and Mn for dry reforming of methane. Catal. Today 384–386, 257–264. https://doi.org/10.1016/j.cattod.2021.03.004.
Wang, P., Wei, S., Wang, S., Lin, R., Mou, X., Ding, Y., 2022b. Interface-directed epitaxially growing nickle ensembles as efficient catalysts in dry reforming of methane. J. Energy Chem. 66, 502–513. https://doi.org/10.1016/j.jechem.2021.08.065.
Wang, M., Zhao, T., Dong, X., Li, M., Wang, H., 2018. Effects of Ce substitution at the A-site of LaNi0.5Fe0.5O3 perovskite on the enhanced catalytic activity for dry reforming of methane. Appl. Catal. B 224, 214–221. https://doi.org/10.1016/j.apcatb.2017.10.022.
Wu, J., Qiao, L.-Y., Zhou, Z.-F., Cui, G.-J., Zong, S.-S., Xu, D.-J., Ye, R.-P., Chen, R.-P., Si, R., Yao, Y.-G., 2019. Revealing the Synergistic Effects of Rh and Substituted La2B2O7 (B = Zr or Ti) for Preserving the Reactivity of Catalyst in Dry Reforming of Methane. ACS Catal. 9 (2), 932–945. https://doi.org/10.1021/acscatal.8b03319.
Yang, E., Moon, D.J., 2017. CO2 Reforming of Methane over Ni0/La2O3 Catalyst Without Reduction Step: Effect of Calcination Atmosphere. Top. Catal. 60 (9–11), 697–705. https://doi.org/10.1007/s11244-017-0779-z.
Zhang, X., Deng, J., Pupucevski, M., Impeng, S., Yang, B., Chen, G., Kuboon, S., Zhong, Q., Faungnawakij, K., Zheng, L., Wu, G., Zhang, D., 2021. High-Performance Binary Mo–Ni Catalysts for Efficient Carbon Removal during Carbon Dioxide Reforming of Methane. ACS Catal. 11 (19), 12087–12095. https://doi.org/10.1021/acscatal.1c02124.
Zhang, M., Zhang, J., Zhou, Z., Chen, S., Zhang, T., Song, F., Zhang, Q., Tsubaki, N., Tan, Y., Han, Y., 2020. Effects of the surface adsorbed oxygen species tuned by rare-earth metal doping on dry reforming of methane over Ni/ZrO2 catalyst. Appl. Catal. B 264, 118522. https://doi.org/10.1016/j.apcatb.2019.118522.
Zhang, M., Zhang, J., Zhou, Z., Zhang, Q., Tan, Y., Han, Y., 2022. Effects of calcination atmosphere on the performance of the co-precipitated Ni/ZrO_2 catalyst in dry reforming of methane. Can. J. Chem. Eng. 100 (S1) https://doi.org/10.1002/cjce.24129.